Laser Powder Bed Fusion of Ti-6Al-4V Alloy

[1]Eyob Ghebreiesus, [2]Amir Mostafaei

[1] Author, BSc. Aerospace Engineering, Illinois Tech
[2] Advisor, Phd. Material Science, Illinois Tech

National Science Foundation Research in collaboration with Illinois Tech
Department of Materials and Additive Manufacturing
10 W 35th St Chicago, IL 60616

August 12, 2021

Abstract

Additive manufacturing (AM) is the process of joining materials to make objects from three-dimensional (3D) model data, usually layer upon layer, as opposed to subtractive manufacturing methodologies. It includes various near-net shaping processes that are capable of building complex 3D geometries directly from raw materials, which require little post processing. This report looks at several types of materials printed using additive manufacturing.The materials used are Ti-64, Inconel-718 and Stainless Steel. The purpose of this report is to explore how Laser Powder Bed Fusion transformed the manufacturing process of different materials. This discipline of process engineering summarizes the broad range of processes, where particles are synthesized, tailored, separated or are used as supporting agent. The characterization of these processes and of the particles thus is key for a detailed understanding. As particles are three- dimensional objects, their morphology as well as the macroscopic structures formed by the particles should be characterized using three-dimensional methods. Using methods of lower dimension often is bound to a loss of information such as a particle size distribution based on a single equivalent diameter, a pore size distribution of a specimen without having the spatial information of the pore network or the stereological bias known in the field of conventional microscopy. Particle technology as sub-discipline of process engineering summarizes the broad range of processes, where particles are syn- the sized, tailored, separated or are used as supporting agent. The characterization of these processes and of the particles thus is key for a detailed understanding. As particles are three- dimensional objects, their morphology as well as the macroscopic structures formed by the particles should be characterized using three-dimensional methods. Using methods of lower dimension often is bound to a loss of information such as a particle size distribution based on a single equivalent diameter, a pore size distribution of a specimen without having the spatial information of the pore network or the stereological bias known in the field of conventional microscopy.

Keywords: AM, EBSD, LPBF, Ti-64, SEM, SLM, XDR, XRD, Microscopy, Keyholes, Porosity

1 Introduction

Additive manufacturing (AM), also known as 3D printing, is a transformative approach to industrial production that enables the creation of lighter, stronger parts and systems. It is yet, another technological advancement made possible by the transition from analog to digital processes. In recent decades, communications, imaging, architecture, and engineering have all undergone their own digital revolutions. Now, AM can bring digital flexibility and efficiency to manufacturing operations. It utilizes data computer-aided-design (CAD) software or 3D object scanners to direct hardware to deposit material, layer upon layer, in precise geometric shapes. As its name implies, additive manufacturing adds a material to create an object. By contrast, when you create an object by traditional means, it is often necessary to remove material through milling, machining, carving, shaping or other means. Although the terms "3D printing" and "rapid prototyping" are casually used to discuss additive manufacturing, each process is actually a subset of additive manufacturing. While additive manufacturing seems new to many, it has actually been around for several decades. In the right applications, additive manufacturing delivers a perfect trifecta of improved performance, complex geometries, and simplified fabrication. As a result, opportunities abound for those who actively embrace additive manufacturing whether in terms of finance, material strength and or uses. In this laboratory-based research we looked at three different materials. They are Titanium-64 alloy, Stainless Steel and Inconel-718 Nickel superalloy. With each to its advantages we'll over what the basic steps for sample design and printing, sample preparation and characterization.

1.1 What is Ti-6Al-4V alloy?

Ti6Al4V alloy, also known as Ti-64 , is an α plus β titanium alloy with high strength, low density, high fracture toughness, excellent corrosion resistance and superior biocompatibility. Recognized as the most popular titanium alloy, Ti6Al4V occupies almost a half of the market share of titanium products used in the world today [1]. Ti6Al4V alloy was originally developed for aircraft structural applications in the 1950s.

The formation of α prime martensite phase is beneficially produced by the rapid cooling through diffusion less transformation while $\alpha + \beta$ transformation is a diffusional process. Conventionally, Ti-6Al-4V consists of a lamellar structure allowing a high strength with slightly reduced ductility. Refinement of the micro-structure results in a higher yield stress. However, after SLM, the microstructure of as-built Ti-6Al-4V commonly consists of a fine α martensitic micro-structure. The high cooling rates during Selective Laser Melting (SLM) result in the formation of the acicular (lamellar) α martensitic phase in Ti6Al4V. Cross-sectional images collected along the SLM building direction show the presence of long columnar grains of prior beta phase (Figure 1. A and B) courtesy of Zhang [2]. Strongly textured structures can lead to significant anisotropic mechanical properties, causing different mechanical responses to external loading along different sample orientations.

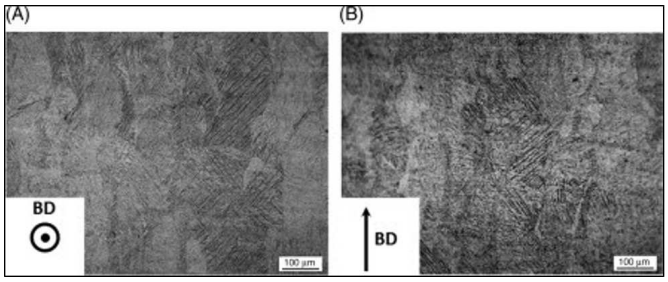

Figure 1: Cross-sectional images collected using SLM.

1.2 Mechanical Properties of Processed Ti-6Al-4V

SLM produces parts with finer microstructures, increasing the mechanical strength (compared to cast Ti-6Al-4V or even sometimes to wrought products). Reported strength values range from about 1000 to 1400 MPa, a 50% increase over wrought products: with corresponding elongations ranging from 25 to 4.4%, respectively. Corresponding hardness values can range between HRC 37 to 54. For example, the coefficient of variation, which represents the ratio of the standard deviation to the average, was up to 48 per cent for elongation at break. Thus, the difference in the mechanical properties of the AM processed samples and the wide scatter among the mechanical properties reported by the different sources, highlight the issue of repeatability and reliability of the mechanical properties of the AM-processed Ti-6Al-4V alloys. According to the standard specifications for wrought Ti-6Al-4V (ELI) and cast Ti-6Al-4V alloys for surgical implant applications (ASTM F136-13 and ASTM F1108-14), the elongation of the material should be at least 8 percent. The content of interstitials has a substantial influence on the mechanical properties of Ti- 6Al-4V. As indicated an oxygen content higher than 0.2 wt.% leads to a higher strength and a lower ductility in the Ti-6Al-4V alloy. A decrease in oxygen and nitrogen content improves the ductility, fracture toughness, stress-corrosion resistance, and resistance against crack growth. As published in the literature, the UTS for SLM Ti-6Al-4V (ELI) horizontal samples varied from 1206 to 1267 MPa.

1.3 Industrial Uses of Ti-64

This lightweight and yet strong alloy saves weight in highly loaded structures and is hence extremely suitable for jet engines, gas turbines and many air frame components. While the aerospace industry still dominates the Ti6Al4V demand, other application fields such as marine, automobile, energy, chemical and biomedical industries have also found its wide acceptance during the last half a century. The low density, high strength, high corrosion resistance and biocompatibility are attractive characteristics of Ti6Al4V for applications such as bridges and dental implants. Its applications have also been extended to the marine and chemical industries due to its high corrosion resistance to most corrosive acids and alkalis.

However, despite the high demand, manufacture of Ti6Al4V products is always challenging due to its poor thermal conductivity, the propensity to strain hardening and active chemical reactivity to oxygen.

1.4 Traditional Manufacturing of Ti-64

Conventional manufacture of Ti6Al4V products relies on forging, casting and rolling of bulk feedstock materials, followed by subsequent machining to final shapes and dimensions. These traditional manufacturing processes always inevitably result in a large amount of material waste, high manufacturing cost and long lead time. Some of the traditional methods are:

Forging: A manufacturing process involving the shaping of a metal through hammering, pressing, or rolling. These compressive forces are delivered with a hammer or die.

Casting: This is a manufacturing process used by the forging industry to produce an object (often metal) of a specific desired shape. This is achieved by pouring hot molten metal into a mold that contains a hollow cavity of the exact required shape.

Extrusion: It's a process used to create objects of a fixed cross-sectional profile. The two main advantages of this process over other manufacturing processes are its ability

to create very complex cross-sections, and to work materials that are brittle, because the material only encounters compressive and shear stresses, such as aluminum, by forcing it to flow through a shaped opening in a die. Extruded material emerges as an elongated piece with the same profile as the die opening.

Coating: The coating process consists of applying a coating material to a moving web of flexible substrate. The carrier substrate may be paper, film, or aluminum foil and the resulting material's additional properties will vary depending on the required application and on the material's end-use. Many industrial coating processes involve the application of a thin film of functional material to a substrate.Industrial coatings are engineered barriers that protect parts from a wide variety of damages and extreme environments

Secondary manufacturing: processes are those processes that are performed after the initial manufacturing process like injection molding, CNC machining production, and so on. As the name implies, these processes involve performing additional work on parts or materials that have already been subjected to a primary machining process. There are many types of secondary machining processes; these can remove unwanted material from a part, refine an existing feature, or produce some other type of enhancement beyond the scope of primary machining. Those processes typically are like welding, grinding, coating, and polishing.

1.5 Additive Manufacturing Technologies

Compared to traditional manufacturing methods, the most significant advantage of AM is its free form fabrication of complex parts directly from feedstock materials without involving traditional manufacturing methods such as extrusion, forging, casting and secondary machining processes to achieve desired shapes. The near-net shaping capability makes AM a cost effective technique since it minimizes wasted material. There are numerous types of AM widely used in present day. Some of those are:

Directed Energy Deposition (DED): In the Direct energy deposition process, the laser beam creates a molten pool, into which the powder material is delivered via argon gas and locally injected to fuse and solidify into a bead. After building one layer, the laser and powder feeding head is raised in Z direction with a preset height and starts building a subsequent layer. The DED process is usually conducted in an inert environment filled with the argon gas where the oxygen level can be controlled to below 5–10 ppm. After deposition, the unused blown out powders can be recycled.

Selective Energy Melting (SLM): An additive manufacturing process in which preplaced fine metal powder is melted by using a high-power laser to generate a layer. Layer by layer, powder is preplaced and melted to generate a part. The technique is also termed powder-bed fusion. During this process, significant remelting of surrounding tracks and layers normally takes place.

Electron Beam Melting (EBM): This is a Rapid Proton capture process, developed and commercialized by Arcam AB in Sweden; it produces fully dense metal parts directly from metal powder, having the characteristic properties of the target material. The EBM system builds structures from the bottom up by scanning the focused electron beam to selectively melt specific powder areas. It reads data from a 3D CAD model and lays down successive layers of powdered material. The process continues until the last layer of the part is built. It takes place under vacuum, which makes it a highly suitable process to fabricate structures using reactive materials that cannot be exposed to the atmosphere. The EBM system is an electron optical system similar to an SEM60 or an EB melting system. The EBM process can build a minimum layer thickness of 0.05mm and it has a tolerance capability of $\pm$ 0.4 mm.

Metal Injection Molding (MIM): Metal injection molding is a manufacturing method that combines traditional PM with plastic injection molding. Over the past decade it has established itself as a competitive manufacturing process for small precision components that would be costly to produce by alternative methods. It can be used to produce comparatively small parts with complex shapes from almost any type of material such as metals, ceramics, inter-metallic compounds, and composites (German, 1984). Recently MIM has been studied not only for hard metals, but also for materials such as titanium, copper, and aluminum (German and Bose, 1997). Unlike in the case of PM, MIM requires mixing metal powders with a large amount of polymeric binder. After this the organic constituents are removed in a de-binding step such as solvent extraction or pyrolysis. The brown body is held in the molded form only by metal powder after de-binding. This de-binding process and powder forming mechanism is unique to the MIM process.

2 Procedure

2.1 Designing Samples

Before printing the samples, you need to design, select the best powder and parameter settings for printing. Designing is usually done using different types of CAD software on a computer. For the Ti-64 samples 31 samples are designed as seeing in Figure 2 and Figure 3 using Netfab Autodesk 2020. Each of these samples have different parameter settings, like power, speed and or pre heat temperature. For the 31 samples we printed all of them were preheated to 200°C. The common feature of these AM processes is the utilization of geometrical data contained in a 3D computer aided design (CAD) file, which is sliced into layers with a defined thickness. While designing the samples, it's best to carefully place each sample with in the base-plates so as to avoid any miss steps by the laser power. Carefully check and note down the appropriate settings and sample placement before proceeding to print.

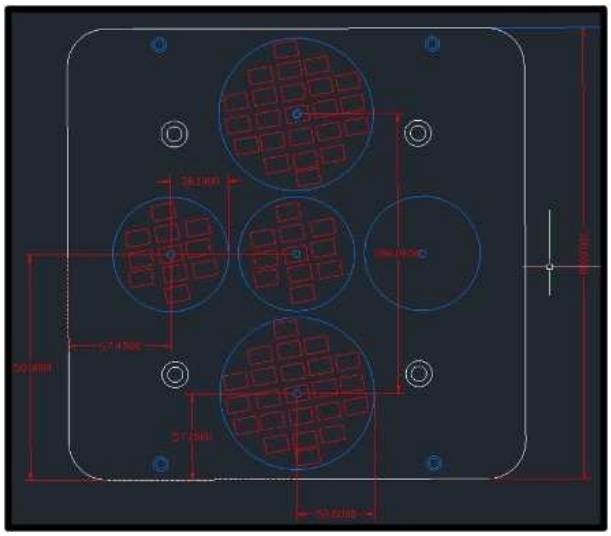

Figure 2: Designing Samples.

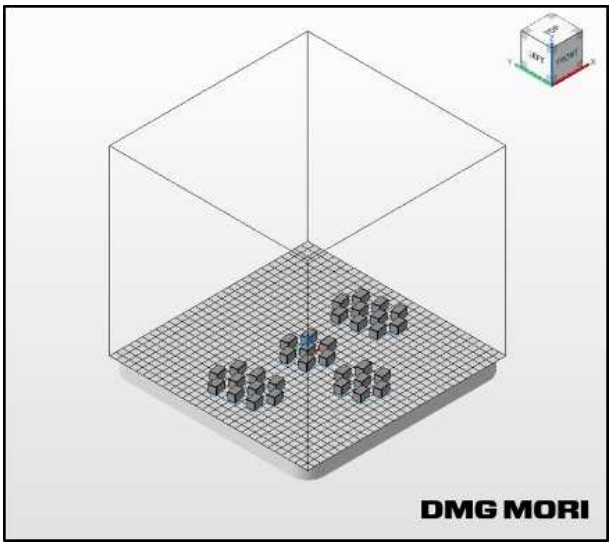

Figure 3: Location of Samples on Base-plate.

After designing the sample layout using software Autodesk Netfab, the settings are uploaded to the LASERTEC 30 SLM in the lab. This machine is a laser-based powder printer that melts and prints the desired sample according to the given parameters. The Powder used is of two types: irregular and regular Ti-64 powder. The goal of the research is to study if the shape of the powder has effect in the mechanical and chemical properties of the Ti-64 samples.All the 31 samples have either a different power setting or scan speed threshold (see Table 1). Those sample parameters are graphed and presented in Figure 4. The plot shows the samples with their respective parameter settings. For example, sample 1 has a laser power setting of 150W and a scan speed of 400mm/s. Similarly, sample 27 has a power 370W and 1500mm/s.

Table 1: Sample Scan Speed and Power values

Sample No	Scan Speed (mm/s)	Laser Power (W)
1	400	150
2	400	225
3	400	280
4	400	340
5	400	370
6	600	150
7	600	225
8	600	280
9	600	340
10	600	370
11	800	150
12	800	225
13	800	280
14	800	340
15	800	370
16	1000	225
17	1000	280
18	1000	340
19	1000	370
20	1250	225
21	1250	280
22	1250	340
23	1250	370
24	1500	225
25	1500	280
26	1500	340
27	1500	370
28	1000	385
29	1250	385
30	800	385
31	1500	385

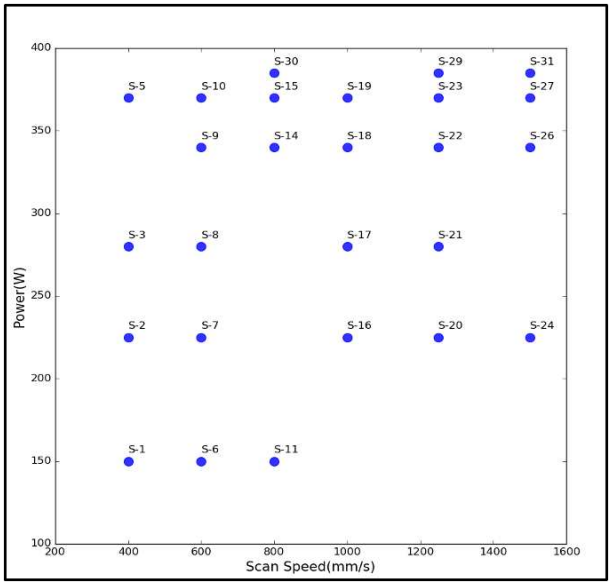

Figure 4: Power vs Scanspeed Plot (S denotes Sample).

The various scan speed and SLM laser power values in Table 1 allows us to study and monitor how laser power and speed affects additive manufacturing. At a letter section, the porosity is compared for each sample and graphed accordingly. It is also good to use more sample parameter in order to avoid sample bias and get accurate results. Having more sample means we can anticipate some samples not being printed due to technical or mechanical issues raised by the SLM machine.

2.2 Printing Samples

Printing samples is done using the Lasertec SLM 30 Machine. It usually takes 4 to 5 hours to print 30 or more samples depending on the parameter settings. It also needs to be checked for preheating process. Preheat is just the warming up the melting chamber to a desired temperature in order to study how the layers are formed and to relieve some stress in powder binding. If a printing process is required for a print process, it should be noted and assessed whilst studying results of the samples later. Useful things before printing is to upload the sample data, rename all the samples, cleaning the baseplates, bring down the oxygen level below 0.08%, check the argon gas levels and sealing the melting chamber. Following the sliced pattern, a focused, high-power laser or electron beam scans and melts the precursor powders, forming a molten pool. As the heating source moves away, the molten pool cools down quickly and solidifies to form a track bead. This process is repeated to successively build new layers until a final geometry is completed.

Once printing is done, all the previous actions should be redone in order to keep the machine to it's initial settings and be ready for cleaning. After the samples are printed (see Figure 5 below) they are taken to a post processing lab to be cut into smaller parts using an Electric Discharge Machining (EDM). EDM is powered through a high electric current that is discharged through a voltage difference in order to cut, split and trim sample parts with high precision. Each sample is cut into two or more parts, so that each is used for different studies. For example, one-part can be used to study Microscopy and Corrosion testing, while the second can be used for FEM and EBSD analysis or even tensile testing as well. Additionally keeping cut-samples in the long run also helps to trace back our studies and replicate it without having to print new ones. This mechanism allows us to save Ti-64 powder.

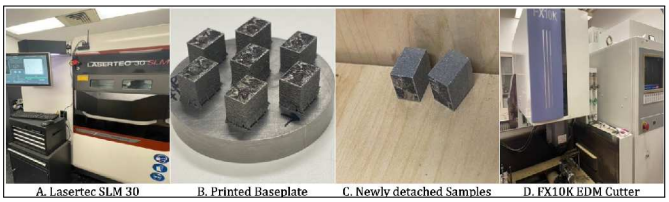

Figure 5: Printing, detaching, and cutting samples.

2.3 Mounting

The next step is to mount the samples so that they are ready for grinding and polishing. Those three steps are necessary in order to take Microscopy, study scratches, check porosity and any other analysis required. Mounting is the just the process of putting the getting part of the sample in a holder resin which makes it easier to grind and polish the sample. There are two types of Mounting see Figure 6 below. Compression or hot mounting presses are used to form and cure compression mounting compounds around a sample. The pressure and heat applied is typically not a problem with most metal alloy, ceramic, glass or inorganic samples. Cold mounting equipment is used to mount samples for microscopy or other analysis using cold or liquid resins. Cold mounting resins are typically a two-part system. A sample is placed in a cold mounting ring mold or dam, mold cup, or rubber molds and then the cold mounting resin is poured around the sample and cured. Some mold rings remain with the sample and cannot be reused. Silicone rubber molds are reusable because the mounting sample can be removed. Curing typically occurs at ambient or room temperatures. Usually engraving is done after mounting the sample. Refer to Figure 6-D to see how engraving is done. The idea is to label your samples so that you can differentiate them easily. Engraving is preferred than writing on your labels using a marker, because the label doesn't wear off easily while grinding or polishing.

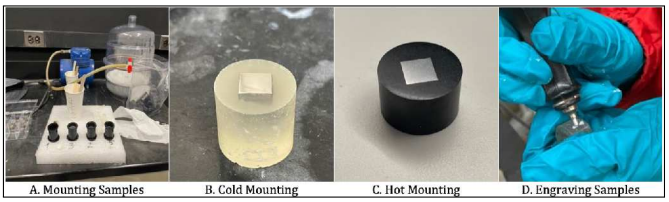

Figure 6: Mounting and labeling.

2.4 Grinding Samples

Grinding is a machining process that's used to remove material from a workpiece via a grinding wheel. As the grinding wheel turns, it cuts material off the workpiece while creating a smooth surface texture in the process. A mechanical process using a rotating grinding wheel made from abrasive material containing small particles of grit ranging from fine to coarse see Figure 7-(A and B). The wheel revolves around a central axis, making contact with the surface of the workpiece, while the particles act as cutting tools that cut chips from the material. There two ways to grind a sample, manual and automatic. These are usually selected based on necessity and efficiency. Grinding needs a sandpaper (grinding paper) with a specific grit size. The grit of sandpapers is a rating of the size of abrasive materials on the sandpaper. The higher grit number is

equivalent to a finer abrasive, which creates smoother surface finishes. Lower grit numbers represent coarser abrasives that scrape off materials much quicker. For those 31 samples printed we started at 240, 500, 600, 800, and then 1200 at the end. You grind each sample until it's smooth, with no scratches and is ready for polishing. Note that a scratch made at a higher grid can only be removed by going one or two steps back to a lower grit number. Thus, if you made a scratch at 1200 grit-size, only an 800 or 600 can remove that scratch. Grinding takes the most time in sample preparation and is extremely tedious.

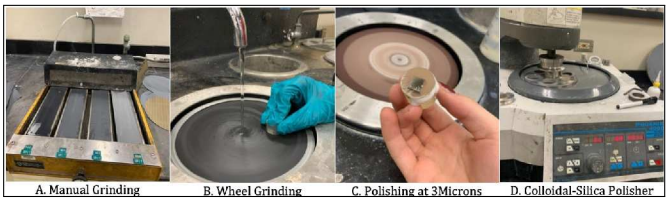

Figure 7: Sample grinding and polishing Process

2.5 Polishing Samples

Polishing is the process of creating a smooth and shiny surface by rubbing it or by applying a chemical treatment, leaving a clean surface with a significant specular reflection. In some materials, polishing is also able to reduce diffuse reflection to minimal values. Technically polishing refers to processes that use an abrasive that is glued to the work wheel, while buffing uses a loose abrasive applied to the work wheel. The two main reasons for polishing are to remove considerable amounts of metal or nonmetallic and smooth a particular surface. Figure 7-(C and D) are prime examples of polishing. Similarly, for polishing is based on the grit size of the polisher paper. We have 9micron, 3microns, 1microns and 0.05microns at last. The lower the number the finer the polishing paper is, and thus the smoother your sample becomes. Mostly polishing is done on a wheel machine. However, at the last process we have a colloidal silica based automatic polisher to finalize the sample polisher. After each grinding and polishing one is supposed to wash the sample using distilled water, methanol, and isopropanol consecutively to clean the sample. Then carefully sonicate the sample using ethanol or methanol for about 3 minutes. Sonication is just the act of applying sound energy to agitate particles in a sample, for various purposes such as the extraction of multiple compounds from plants, microalgae, and seaweeds. In this laboratory, it is usually applied using an ultrasonic bath or an ultrasonic probe, colloquially known as a Sonicator.

Now that the samples are done, they're all ready for analysis whether it's Microscopy, SEM or EBSD. Note that sometimes the samples can get scratched due to hand placement, touching, or scrabbing against any surface. You need to be careful to not scratch it. But if at point they get scratched follow the same process for grinding and polishing in order to smoothen the surface again.

3 Results and Analysis

After the samples are prepared, we move to the first analysis that is Microscopy. We look at sample scratches, porosity and other defects using microscopy. Porosity refers to the level of solidity achieved in an additively made metal part, that is, whether there are cavities or holes between the layers of a sample part. During printing the laser is used to melt a layer of metal powder to the point where the powder liquefies and adheres to an earlier melted layer. Usually, this process results in very dense parts, typically 98% dense or more. However, there are times when the melt is not complete, resulting in hollows or cavities, also referred to as porosity. The two types of porosity are lack of fusion porosity and gas porosity. The fundamental origin of lack-of-fusion porosity is insufficient overlap of successive melt pools. The approach allows rapid prediction of the effects of changes in processing parameters (beam power and beam speed, hatch spacing and layer thickness) on part porosity. On the other hand, gas porosity occurs because the molten metal can hold a large amount of dissolved gas, unlike the solid form. This occurs when the molten metal is cooled down too quickly. That causes the gases to be trapped and thus they form bubble like circle dark spots on the sample. Gas porosity can be eliminated through good design, better parameter settings, and sometimes using hot isostatic process. The goal of microscopy is to optimize the processing parameters in order to reduce porosity as much as possible. Now this can be whether gas porosity or lack of fusion porosity. The main goal of this research is to come up with the best possible parameter setting for printing. The research aims to avoid porosity as much as possible. Because porosity can create little defects which in return become a big problem during manufacturing. Porosity can remain an issue even after doing every possible action to avoid it. Traditionally a major issue has to do with the printer itself, die-cast components, microscopic holes form within a part's body during the AM process. Though invisible to the eye, they reduce component density, potentially leading to cracks, leaks, and fatigue. In applications with pressure differentials or requirements to be air or fluid tight, for example in cooling systems, this can be an especially critical issue.

3.1 Microscopy

Looking down a reflection microscope we see the light reflected off a sample. The contrast can arise in different ways. Transmission light microscopes are used to look at thin sections – the specimen must transmit the light. The specimen is mounted and placed on the stage; begin by slowly increasing the power of the light source until there is a bright spot visible on the sample. With the lowest mag-

nification lens in place focus using the coarse focus knob: without looking down the microscope, lower the objective lens close to the specimen surface, and then use the coarse focus knob to slowly raise it until the circle of light on the specimen appears reasonably sharp. Now, looking through the eyepiece, adjust the coarse focus control. When looking down the eyepiece and using coarse focus, we should only ever adjust so as to move the sample away from the objective. To increase the magnification, slide the rotatable nosepiece around (ensuring the lens does not touch the specimen) and then re-focus using the fine focus (it should take very little adjustment!). Once a representative area is found and focused a digital camera can be used to take a photo and a sketch can be made. After taking the images, stitching, and fusing is needed. This is done usually through a third-party software called ImageJ or Fiji-ImageJ. It's a public domain Java image processing program. ImageJ is used to display, annotate, edit, calibrate, measure, analyze, process, print, and save raster (row and column) image data. ImageJ is used in various other scientific disciplines as well. It has the potential to be a powerful tool for any field that benefits from image visualization, processing, and analysis: earth sciences, astronomy, fluid dynamics, computer vision, signal processing, etc. Based, on the selection type, calculates and displays either area statistics, line lengths and angles, or point coordinates. Area statistics are calculated if there is no selection or if a sub-region of the image has been selected using one of the first four tools in the toolbar.

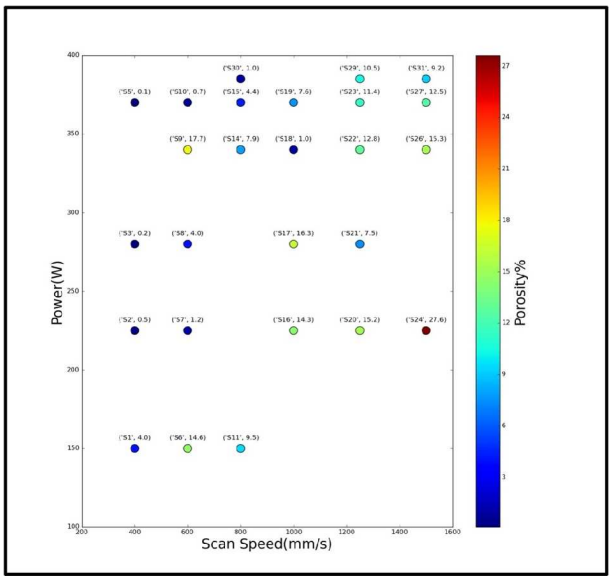

Figure 8: Porosity % using Microscopy.

Out of the 31 samples printed, we were able to do ImageJ analysis on 26 of the samples. Five of the samples came out badly due to the technical issues as discussed earlier. We looked at the porosity and density area against the parameter (Speed and Power) settings we set initially for these 26 samples. The results are plotted on Figure 8. The plot is provided using a free third-party software Python. As usual the codes are provided on the official GitHub for this project and can be referred at any time. The colors indicate the amount of porosity in the samples. Red is used as a higher indication of porosity, while blue is the least. Each point on the plot represents a sample number and the amount of porosity it contains. For example Sample 24 (S24, 27.6) is found to contain the most porosity which we intend to avoid. It shows that at a higher laser scan speed there's lack of fusion porosity forming on the layers of the samples. And when there's a lower laser-power involved with higher scan speed the greater the porosity %. A porosity of 27% for a sample is usually unwanted, and best if avoided.

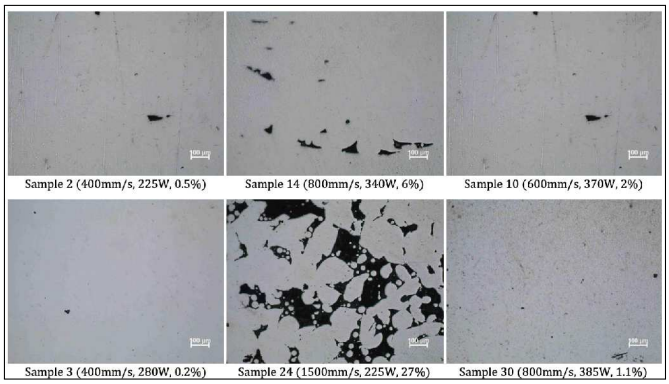

Figure 9: Surface porosity comparison.

We can see the surface comparison in Figure 9 very well. The idea of porosity is illustrated by frames of images from the selected given sample. One can notice that the higher scan speed leads to lack of fusion porosity. Comparing Sample 24 with Sample 2, there's an obvious relation between scan speed and porosity. Thus, the microscopy analysis can tell us which parameters to avoid (in this case a 1500mm/s and 225W) and which ones to select as for the best printing results. It shows the best parameter settings are found on the center of plotted graph in Figure 8. Furthermore, one can see the blue light samples around the mid-top center of the plot have relatively low porosity when compared. Once donw with microscopy, we looked at X-ray Diffraction analysis, Scanning Electron Microscope, Field Emission -SEM, Corrosion testing, Mechanical testing, Digital X-ray Radiography analysis.

3.2 Scanning Electron Microscope

A scanning electron microscope (SEM) scans a focused electron beam over a surface to create an image. The electrons in the beam interact with the sample, producing various signals that can be used to obtain information about the surface topography and composition. Because of its great depth of focus, a scanning electron microscope is the

EM analog of a stereo light microscope. It provides detailed images of the surfaces of cells and whole organisms that are not possible by normal microscope [3]. It can also be used for particle counting and size determination, and for process control. It is termed a scanning electron microscope because the image is formed by scanning a focused electron beam onto the surface of the specimen in a raster pattern. In the lab there are two types SEM's. One is the standard SEM and the second is the Field Emission SEM (FE-SEM). For the analysis of FE-SEM we used as built Ti-64 sample with Hot Isostatic Pressure (HIP) treatment. Figure 10 shows the results of FE-SEM provided by the research lab.

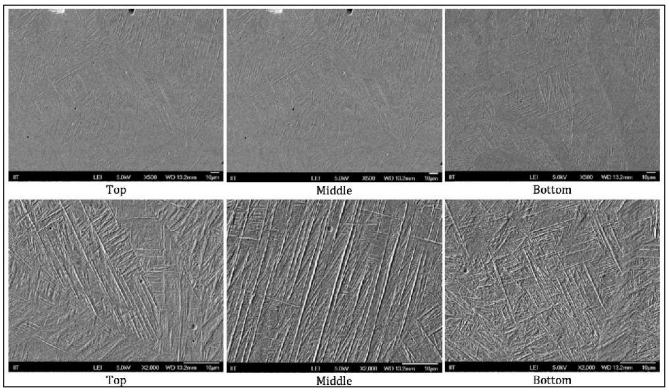

Figure 10: SEM images First row images have 500x magnification, while the second row have 2000x.

The SEM images are taken from top to bottom in a vertical cut. Three images are taken generally: top, middle, and bottom. As shown in the above figure 10, the first row is images takes at 500x magnification. Although we can't see the sharp lines, but we can see the surface of the sample in much detail. However, the second row shows us the phases of the sample material even. They are magnified at a scale of 2000x. Clear white sharp lines are observed in the sample. Those are the alpha prime () phases of Ti-6Al-4V. They give the sample it's strength. Essentially an SEM images can tell you about the mechanical properties of the sample at hand. And in this case the SLM printed Ti-64 samples have similar strength values as those traditionally produced samples.

3.3 Dynamic X-ray Radiography

The third analysis conducted was the Dynamic X-ray Radiography. DXR is used to measure Keyholes (see Figure 11. Courtesy of C. Zhao [4]) and other properties of a sample. One way to minimize the effects of boundary layers along walls on the measured kinematics is the use of X-ray radiography, the building block of X-ray CT. For example, X-ray radiography has long been used to inspect density variations in a variety of geoscientific problems, including inferences about the existence of discontinuities in sandstones and clays in stationary samples and measuring density in granular materials. We were able to obtain DXR images of Ti-64 printed using an irregular powder at the Argonne National Laboratory in Illinois. Keyholes are a small key shaped holes in a printed sample. They're caused by a strong recoil pressure from the rapid evaporation of metal pushing the melted liquid down. This creates a deep and narrow cavity called a keyhole. Sometimes keyholes can largely enhance laser absorption and improve energy efficiency. However, usually the keyhole walls constantly fluctuate and collapse that creating pores and leads to defects. This occurs when bubbles of gas get trapped underneath the surface a part constructed during the metal additive manufacturing process, resulting in the formation of relatively spherical pores under the surface of the part. This is opposed to other types of porosity, which can form from incomplete melting of the powder material or improper adhesion of two layers of material.

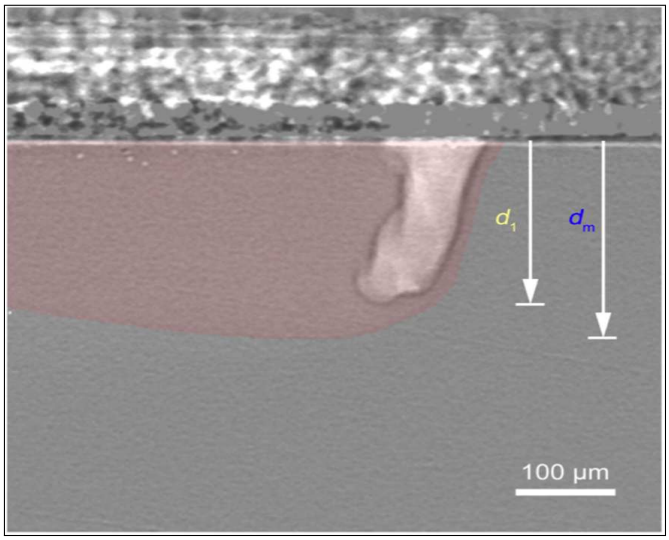

Figure 11: A keyhole observed using DXR.

In total 5 samples were sent to Argonne to be printed. All 5 samples have same laser power of 350W and a frequency frame rate of 50kHz but with different scan speeds as seen in Table 1. The scan speed ranges from 400mm/s – 1200 mm/s. The purpose of XRD analysis is to see how much scan speed alone has an effect in the creation of the keyhole, and how large or deep the keyholes are generally. A complete data sheet is provided at the appendix of this report. A handful explanation of the graph codes is also posted on GitHub.

To compare the severity of keyhole porosity formation, we used area under the surface of the sample with ImageJ and measured the area faction which displayed keyhole porosity. Measuring Keyhole depth is a little different from measuring porosity. One would have to individually measure the depth until each tiff file frame is finished. And the longer the longer the sample length, the more measuring it

Table 2: Average keyhole depth

Sample No:	Scanspeed (mm/s)	Average depth (μm)	Variance 100
1	400	303.50	23.35
2	500	264.12	13.54
3	600	222.12	11.33
4	700	144.94	8.57
5	1200	46.29	7.90

requires on ImageJ. The high-speed x-ray imaging makes it possible to observe the pore formation process within the keyhole. Regardless of laser power and the presence or absence of powder, pore formation occurs when the bottom tip of a letter 'J' shaped keyhole was pinched off, released at high speed toward the wake of the laser beam, and trapped by the solidification front. With decreasing laser power, the keyhole porosity boundary becomes increasingly sensitive to scan speed, particularly in the presence of powder, and appeared to asymptote to a threshold in power. As seen in Figure 12 the sample with 400mm/s contains big fluctuation but longer average keyhole depth. On the contrary the sample with 1200mm/s was found to have shorter constant keyhole depth. This would only mean one thing i.e., as the scan speed increases, the average depth of the keyhole decreased. In addition to that the variation of keyhole depth increased strongly with decreasing scan speed as seen in Table 2. Compared to sample 1, sample 5 had a much better variance on the average of the keyhole depth. That indicates the accuracy while measuring the keyhole depth. The less fluctuation theirs is the smaller the variance. This is an obvious read in the Figure 12. The blue lines sample 1 have more difference between each point than there's for red points in sample 5.

Compared with bare plate samples, in which such pores tend to merge quickly into the subsequent growing keyhole and disappear, the larger keyhole fluctuations in powder bed samples create sufficient waiting time for the pores. These pores are nearly stationary after pinching off the keyhole and suspended inside the melt pool (or potentially accelerated by the local melt flow through forces such as drag away from the keyhole) to be pinned by the advancing solidification front. Typically, at a constant laser power, keyhole pores form only when the keyhole depth is larger than a threshold, as depicted in the graph in the previous slide. This threshold increases, statistically, with scan speed and laser power in distinct power-law forms respectively. Similarly, an irregular shaped powder leads into a smaller depth keyhole. This is beneficial when comparing the cost of regular vs. irregular powder of Ti-64 alloy. That would mean the production of Ti-64 alloys will much cheaper, defect free and less prone to fatigue creeps.

In the keyhole porosity regime and far away from the keyhole porosity boundary, large pores (i.e., pore size comparable to keyhole length) can be trapped directly by the solidification front while or after pinching off the keyhole.

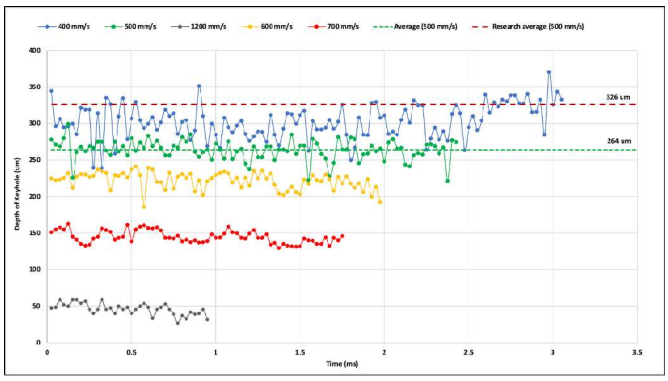

Figure 12: Keyhole depth vs Time.

In this sort of cases, acoustic waves may still exist, but may not play a critical role in driving the pore formation and motion (pore splitting is still possible) because the far side of the pore to the keyhole is pinned by the solidified structure. There's also the concept of acoustic waves in keyhole formation. Acoustic waves could generate from the collision of keyhole walls, the crashing of liquid on the melt pool boundary. For the measurement of acoustic waves, coupling real-time passive acoustic sensing with x- ray imaging may allow one to identify the characteristic signals of those waves relevant to the keyhole pore formation [4]. Indirectly, ultrahigh-speed x-ray diffraction using synchrotron or future high-energy high-repetition-rate free-electron laser sources may also

3.4 X-ray Diffraction (XRD)

X-ray diffraction (XRD) is a nondestructive technique that provides detailed information about the crystallographic structure, chemical composition, and physical properties of materials. It is a technique used to find out the nature of the materials as crystalline or amorphous. It will define the quantification of cementitious materials [5]. It also provides information on structures, phases, preferred crystal orientations (texture), and other structural parameters, such as average grain size, crystallinity, strain, and crystal defects. XRD peaks are produced by constructive interference of a monochromatic beam of X-rays scattered at specific angles from each set of lattice planes in a sample. The peak intensities are determined by the atomic positions within the lattice planes. Consequently, the XRD pattern is the fingerprint of periodic atomic arrangements in a given material. An online search of a standard database for X-ray powder diffraction patterns enables quick phase identification for a large variety of crystalline samples. This means that structural changes induced in a crystalline material by blending with other materials can be monitored using the XRD technique. For this research a nickel superalloy named Inconel-718 was subjected to an XRD analysis. The sample was horizontally cut hipped at 200Mpa for 90minutes (see Figure

13). Inconel 718 is a high strength nickel base superalloy used for cryogenic temperatures up to long term service at 1200°F. The super alloy is used for gas turbine engine parts, firearms production, liquid fuel rocket motor components, springs, fasteners and cryogenic tanks. The idea of this analysis was to understand and graph XRD data using MATLAB in order to determine the samples character fingerprint.

This XRD relation is given by Bragg's Law as:

$$n\lambda = 2d\sin\theta \tag{1}$$

where:

- n is an integer
- λ is the wavelength of the x-ray,
- d is the spacing of the crystal layers (path difference),
- θ is the incident angle (the angle between incident ray and the scatter plane)

Equation 1 is commonly known as Bragg's Law. The law states that when the x-ray is incident onto a crystal surface, its angle of incidence, will reflect back with a same angle of scattering, θ And, when the path difference, d is equal to a whole number, n of wavelength, a constructive interference will occur.

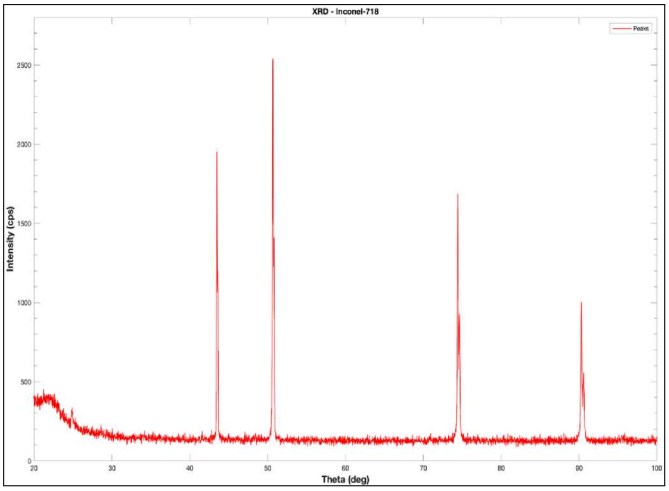

Figure 13: Inconel-718 Hipped at 200MPa for 90 min.

For this super alloy there are four main peaks, and very small peaks associated with the sample in Figure 13. The main peak occurs around 55 degrees for an intensity of 2880 cps, but we need to divide the angle by two and our ideal angle is actually 27.5 degrees.

3.5 Electron Backscatter Diffraction (EBSD)

Electron Backscatter Diffraction (EBSD) is a scanning electron microscope (SEM) based technique that gives crystallographic information about the microstructure of a sample. In EBSD, a stationary electron beam interacts with a tilted crystalline sample and the diffracted electrons form a pattern that can be detected with a fluorescent screen. The diffraction pattern is characteristic of the crystal structure and orientation in the sample region where it was generated. Hence the diffraction pattern can be used to determine the crystal orientation, discriminate between crystallography of different phases, characterize grain boundaries, and provide information about the local crystalline perfection. EBSD has become a well-established accessory for the SEM, which is used to provide crystallographic information routinely [6]. As a result, EBSD is now being applied in numerous different application areas to assist in materials characterization, as shown in the graph. For this research, an EBSD analysis was done for the Inconel-718 hipped at 200MPa for 90minutes. But this time the sample was vertically cut in order to study its phases. A total of 4 sample properties were observed through the EBSD. Using EBSD we were able to study the grain boundary, and surface angles across the sample.

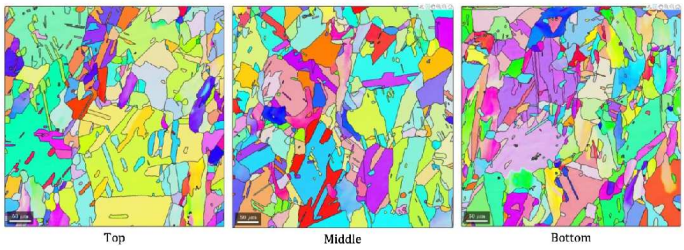

Figure 14: Crystal Orientation map of Inc-718 EBSD

The first three images being analyzed are the crystal orientation map of Inc-718. Figure 14 illustrates the orientations. These maps are derived by EBSD, are often displayed in so-called inverse pole figure (IPF) coloring. These maps (often three maps are displayed for reference direction X, Y and Z) really reflect the locally discovered orientation. They insert additional symmetries which reflect a higher symmetry and therefore perhaps another not-symmetry-equivalent crystal orientation. A grain is a three-dimensional crystalline volume within a specimen that differs in crystallographic orientation from its surroundings but internally has little variation. Grain size is an important characteristic used in understanding the development, engineering, and potential failure in materials. EBSD has a lot of advantages and has become an attractive manufacturing method to produce the super alloys. The experimental results, the beam scanning speed did show notable effects on the preferred orientation of the phase in the Z-plane which presents a relatively strong texture. However, with the increase of the beam speed, the intensity of the texture in the Z-plane decreases first and then increases slightly. Generally, the parts did not show out-

standing anisotropic characteristics in hardness and elastic modulus. The Inc-718 did present the highest properties (Vickers hardness and elastic modulus) between the four parts, which results from its finest microstructure and the weakest texture. In grain boundary engineering it can

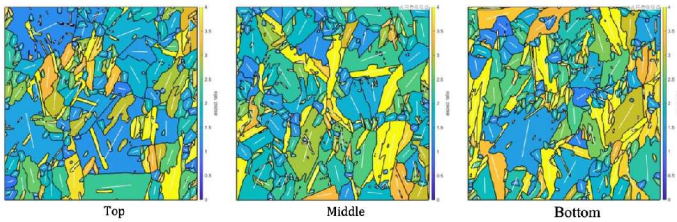

Figure 15: Preferred orientation map of Inc-718 EBSD

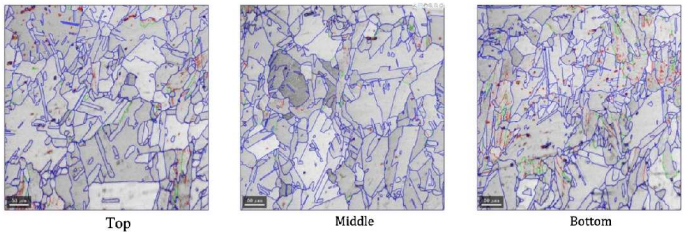

Figure 16: Grain boundaries of Inc-718 EBSD

be important to enhance or reduce the relative abundance of certain grain boundary types in order to optimize the properties of the final material. EBSD is well suited to extract this type of information as it gives both statistical and spatial information about the grain boundaries. Figures 15 and 16 show us the grain boundaries of Inc-718. For that sample, some smooth boundaries are seen in the center, most of them close to a circle. The more circular the boundary the better the strength of the sample is. This meant the sample can withstand cracks, and helps minimizing bending, and sudden fracture.

Figure 17 first row is the Kernel Average Misorientation (KAM), and the second row is Grain Average Misorientation (GAM). The idea to use these local orientations for other applications later arose since first it became obvious that one can link the local position AND the orientation to extract additional but still not evaluated information like the definition of grains as "volumes" of identical orientations. Kernel average misorientation (KAM) during electron backscatter diffraction (EBSD) analysis can be. used as a measure of local grain misorientation. KAM quantifies the average misorientation around a. measurement point with respect to a defined set of nearest neighbor points. Similarly the normal and inverted poles of INc-718 is mapped in Figure 18.

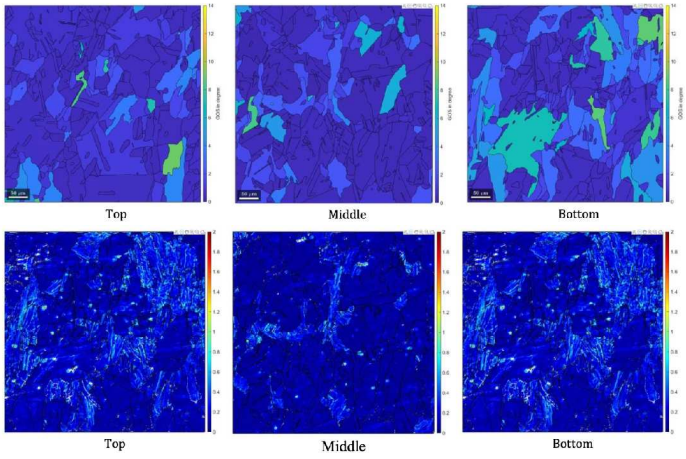

Figure 17: Grain Orientation Spread of Inc-718 EBSD

4 Conclusion

Laser powder bed fusion is a dominant metal 3D printing technology. However, porosity defects remain a challenge for fatigue-sensitive applications. Some porosity is associated with deep and narrow vapor depressions called keyholes, which occur under high-power, low-scan speed laser melting conditions. In this paper, the recent progress on Ti6Al4V fabricated by three mostly developed additive manufacturing (AM) techniques-directed energy deposition (DED), selective laser melting (SLM) and electron beam melting (EBM)-is thoroughly investigated and compared. High-speed x-ray imaging enables operando observation of the detailed formation process of pores in Ti-6Al-4V caused by a critical instability at the keyhole tip. A research by conducted by C. Zhao's team showed [4] similar results to ours, and they found that the boundary of the keyhole porosity regime in power-velocity space is sharp and smooth, varying only slightly between the bare plate and powder bed. The critical keyhole instability generates acoustic waves in the melt pool that provide additional yet vital driving force for the pores near the keyhole tip to move away from the keyhole and become trapped as defects. Fundamental knowledge is provided for the creation of links between processing parameters, resultant microstructures and associated mechanical properties. Room temperature tensile and fatigue properties are also reviewed and compared to traditionally manufactured Ti6Al4V parts. The presence of defects in as-built AM Ti6Al4V components and the influences of these defects on mechanical performances are also critically discussed.

The research also found that porosity increases with higher scan speed but lower laser power. Lack of fusion porosity was observed on samples printed for the Ti-64 samples. Furthermore, Keyhole depth are related with scan speed in the opposite manner. Faster scan speeds reduce the creation of melt pool and show the keyhole depth

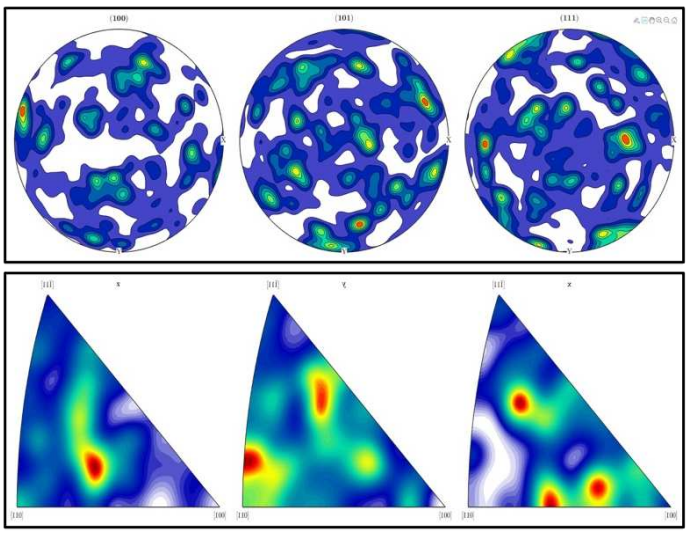

Figure 18: Normal and Inverted poles of Inc-718

is short enough. The propagation of an internal fatigue crack in Ti–6Al–4V was non-destructively observed by synchrotron radiation imaging to clarify the crack growth rate in very high cycle fatigue. The results show irregular powder does have an advantage in decreasing the keyhole depth and increase the strength of the sample. Figure 11 also shows samples printed using an irregular powder are less prone to fatigue crack and produce slighter lesser gas porous compared to regular powder.

This paper aims at illustrating the potential of X-ray tomography for studying the mechanical behavior of materials through various experiments. Typical experimental are the ones which use laboratory and synchrotron X ray sources as shown in the report. Advantages and limitations of all types of sources are presented. Dedicated experimental devices which allow deformation and/or temperature changes to be applied to various types of materials are described. Examples of results of in situ mechanical experiments are presented and discussed in a manner of graphs and images.

For this superalloy there are four main peaks, and very small peaks associated with the sample in Figure 12. The main one occurs around 55 degrees. But since this is twice the theta value, therefore we need to divide it by two. Thus, the actual diffraction angle for the biggest is actually 27.5 degrees. For sample Inc-718, some smooth boundaries are seen in the center, most of them close to a circle. The more circular the boundary the better the strength of the sample is. This meant the sample can withstand cracks, and helps minimizing bending, and sudden fracture. The overall goal of this research was to learn and understand the uses of X-ray imaging in additive manufacturing technology. It provides a great deal of knowledge, hands on experience, and technology to conduct a scientific experiment in the institute. This was only possible through the funds from the National Science Foundation. This research is a great achievement and an eye-opening journey from the start to finish.

References

[1] S. Liu and Y. C. Shin, "Additive manufacturing of Ti6Al4V alloy: A review," *Materials and Design*, vol. 164, p. 107 552, 2019, ISSN: 18734197. DOI: 10.1016/j.matdes.2018.107552. [Online]. Available: https://doi.org/10.1016/j.matdes.2018.107552.

[2] B. Zhang, R. Seede, L. Xue, K. C. Atli, C. Zhang, A. Whitt, I. Karaman, R. Arroyave, and A. Elwany, "An efficient framework for printability assessment in Laser Powder Bed Fusion metal additive manufacturing," *Additive Manufacturing*, vol. 46, p. 102 018, 2021, ISSN: 22148604. DOI: 10.1016/j.addma.2021.102018. [Online]. Available: https://doi.org/10.1016/j.addma.2021.102018.

[3] T. Leißner, A. Diener, E. Löwer, R. Ditscherlein, K. Krüger, A. Kwade, and U. A. Peuker, "3D ex-situ and in-situ X-ray CT process studies in particle technology – A perspective," *Advanced Powder Technology*, vol. 31, no. 1, pp. 78–86, 2020, ISSN: 15685527. DOI: 10.1016/j.apt.2019.09.038.

[4] C. Zhao, N. D. Parab, X. Li, K. Fezzaa, W. Tan, A. D. Rollett, and T. Sun, "Critical instability at moving keyhole tip generates porosity in laser melting," *Science*, vol. 370, no. 6520, pp. 1080–1086, 2020, ISSN: 10959203. DOI: 10.1126/science.abd1587.

[5] F. Yoshinaka, T. Nakamura, S. Nakayama, D. Shiozawa, Y. Nakai, and K. Uesugi, "Non-destructive observation of internal fatigue crack growth in Ti–6Al–4V by using synchrotron radiation μCT imaging," *International Journal of Fatigue*, vol. 93, pp. 397–405, 2016, ISSN: 0142-1123. DOI: https://doi.org/10.1016/j.ijfatigue.2016.05.028. [Online]. Available: https://www.sciencedirect.com/science/article/pii/S0142112316301360.

[6] X. Wang and K. Chou, "EBSD study of beam speed effects on Ti-6Al-4V alloy by powder bed electron beam additive manufacturing," *Journal of Alloys and Compounds*, vol. 748, pp. 236–244, Jun. 2018, ISSN: 09258388. DOI: 10.1016/j.jallcom.2018.03.173.